

Kurzbericht an die Hamburger Krebsgesellschaft e.V.

Abschlussbericht zum Projekt

“Molekulare Mechanismen der PARP-Inhibitor-Resistenz in BRCA1/2-defizienten Tumoren: Identifizierung von Biomarkern der erworbenen Resistenz“

Von

PD. Dr. Wael Mansour

In Vorbereitung auf die geplante Publikation wurde der Abschlussbericht in englischer Sprache abgefasst.

Background

PARP inhibitors (PARPi) are powerful therapeutic tools (i) as mono-therapy in the management of BRCA-associated cancers. The selective targeting of BRCA-deficient cancer cells by PARPi, as a monotherapy, demonstrates the concept of synthetic lethality. Mechanistically, inhibition of PARP1 results in accumulation of unrepaired SSBs, which stall ongoing replication forks generating double strand breaks (DSBs). Such replication-associated DSBs are by homologous recombination (HR). Therefore, inhibition of PARP1 is synthetically lethal with deficiency of either BRCA1 or BRCA2, because of their critical role in HR.

Acquire resistance is developed after several PARPi treatment cycles. There are many described potential mechanisms of resistance to PARPi in cancer cells, including (i) Restoration of HR capacity; (ii) bypassing replication fork perturbations; (iii) increased cancer stem cell population; (iv) decreased levels or activity of PARP1; (v) reactivation of BRCA by reversed mutations and (vi) decreased intracellular availability of PARPi. Therefore, it would be necessary to assess the status of these controlling factors before beginning the treatment with PARPi. A thorough understanding of different mechanisms for the resistance to PARPi will permit us to design better PARPi monotherapy as well as combination therapy, and will allow us to identify conditions that can re-sensitize tumor cells to PARPi; and thus treat cancer patients more efficiently.

Project aim

Overall, the current project aims to study the mechanism(s) underlying the resistance to PARPi in BRCA-deficient tumors. It was aimed to identify some molecular biomarkers that might be used as predictors or modulators for the response/resistance of tumors to PARP inhibition.

Summary

Based on our data, we present protection of DSB ends against end resection process is a key mechanism of PARPi resistance. Several factors have been reported to limit DSB end resection including the DNA damage response factors 53BP1 and its downstream target RIF1. We showed depletion of either of the aforementioned factors would rescue HR in BRCA1-deficient cells and with that drives a resistance to PARPi and MMC.

Here, we identified another factor; namely RAP80, which efficiently limits DSB end resection and hence reactivate HR repair mechanism in BRCA-deficient cells. Importantly, we propose a novel RAP80's role that is BRCA1-independent in limiting end resection through targeting EXO1 to ubiquitin mediated proteasome degradation. Briefly, RAP80 binds directly through its UIM domain to EXO1 which preserves its ubiquitination and hence targeting EXO1 to proteasome degradation.

Results

RAP80 is a limiting factor for DSB end resection step

As illustrated in Fig.1 and in line with its inhibitory effect on DSB end resection step, we reported a significant increase in the recruitment of the endonuclease CtIP upon depletion of RAP80 after 2Gy. The extent of CtIP recruitment increase upon RAP80 depletion was similar to that upon 53BP1 knockdown (Fig. 1B). Consequently,

the recruitment of RPA and RAD51 were significantly decreased in RAP80-or 53BP1- depleted cells (Fig. 1 C&D). In contrast, depletion of BRCA1 decreased CtIP (Fig. 1B), RPA (Fig. 1C) and RAD51 (Fig. 1D) recruitment. Since RAP80 appeared to suppress end resection, which is the prerequisite step for conducting HR.

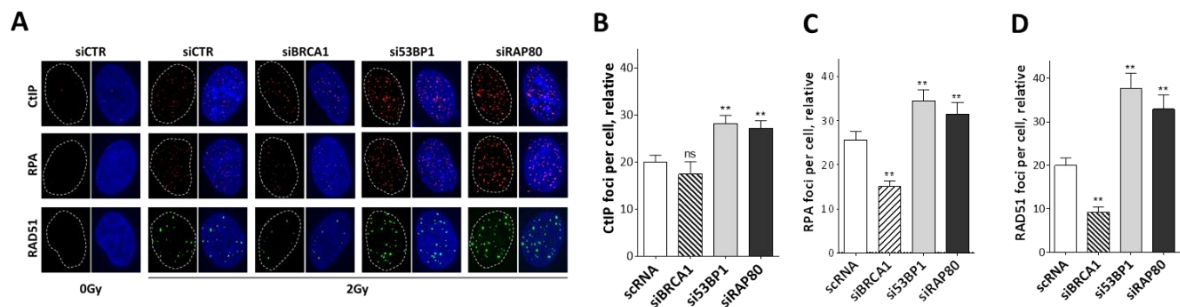


Fig. 1 RAP80 is a limiting factor for DSB end resection step. BRCA1, 53BP1 or RAP80 was depleted in A549 cells using siRNA before irradiation with 2Gy. (A) Representative micrographs for CtIP, RPA and RAD51. (B-D) Quantitation of the experiment in A. In all cases, the number of foci measured in non-irradiated cells was subtracted (relative). Shown are means \pm SEM of at least three independent experiments. Significance is indicated as ns for not significant, * for the $P < 0.05$, ** for $P < 0.001$.

RAP80 depletion rescues CtIP, RPA and RAD51 recruitment in BRCA1-deficient cells.

In order to further test the RAP80's role in limiting end resection, BRCA1 and RAP80 were efficiently depleted either individually or combined in A549 cells and the effect on the recruitment of CtIP, RPA and RAD51 after 2Gy were analysed using IF (Fig. 2A).

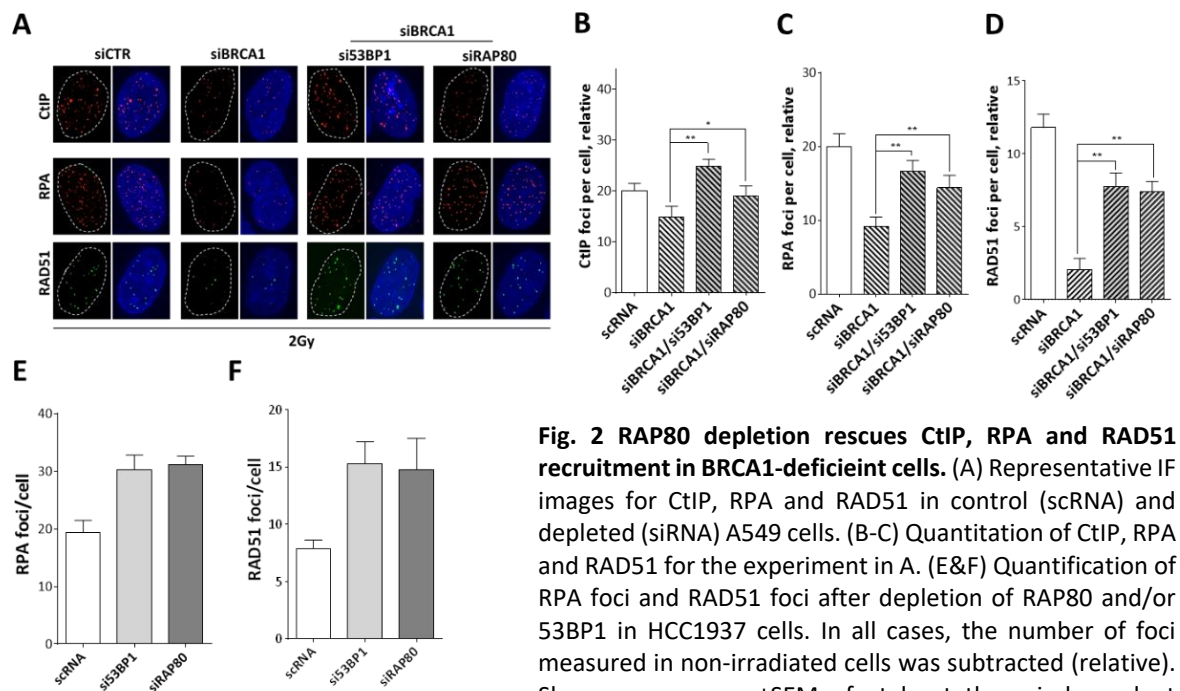


Fig. 2 RAP80 depletion rescues CtIP, RPA and RAD51 recruitment in BRCA1-deficient cells. (A) Representative IF images for CtIP, RPA and RAD51 in control (scrNA) and depleted (siRNA) A549 cells. (B-C) Quantitation of CtIP, RPA and RAD51 for the experiment in A. (E&F) Quantification of RPA foci and RAD51 foci after depletion of RAP80 and/or 53BP1 in HCC1937 cells. In all cases, the number of foci measured in non-irradiated cells was subtracted (relative). Shown are means \pm SEM of at least three independent experiments. Significance is indicated as ns for not significant, * for the $P < 0.05$, ** for $P < 0.001$.

As expected, BRCA1 depletion decreased the number of loaded CtIP (Fig. 2B), RPA (Fig. 2C) and RAD51 (Fig. 2D). Intriguingly, further depletion of RAP80 in BRCA1-knockdown A549 cells rescued the recruitment of CtIP, RPA, and RAD51, indicating a possible BRCA1-independent role for RAP80 in limiting end resection. Consistently, depletion of RAP80 in BRCA1-deficient HCC1937 cells significantly increased the number of RPA and RAD51 foci post-2Gy (Fig. 2E&F). The extents of the rescue mediated by RAP80-knockdown were similar to that obtained

upon depletion of 53BP1 in A549 as well as HCC1937 cells. Together, it is conceivable that RAP80 can work independently of BRCA1 to limit DSB end resection.

Synergistic increase end resection upon co-depletion of RAP80 and 53BP1.

Next we sought to identify the mechanism underlying the BRCA1-independent RAP80'role in limiting DSB end resection. Firstly, we excluded the involvement of 53BP1 in this role by showing that (i) the recruitment of RAP80 does not depend on 53BP1 (data not shown) and (ii) individual depletion of either 53BP1 or RAP80 led to significant increase in the number of recruited CtIP (Fig. 3A), RPA (Fig. 3B) and RAD51 (Fig. 3C) after 2Gy, but more importantly, simultaneous depletion of RAP80 and 53BP1 led to a synergistic increase in the IR-induced recruitment of the aforementioned DNA repair factors. Collectively, we interpret these findings as showing that 53BP1 and RAP80 are working, at least partly, independently in regulating DSB end resection.

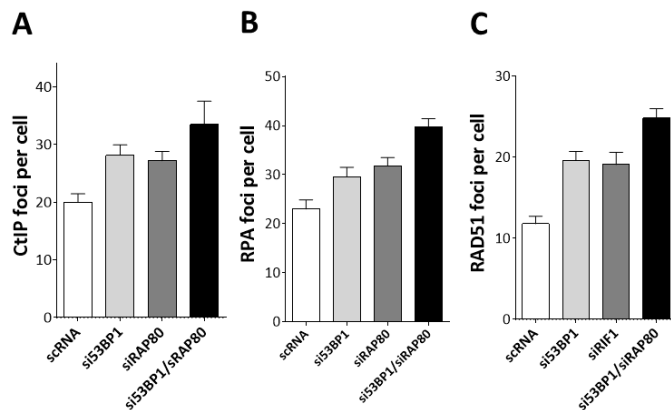


Fig. 3 Synergistic increase end resection upon co-depletion of RAP80 and 53BP1. Quantification of the (A) CtIP, (B) RPA and (C) RAD51 foci in control (scRNA), 53BP1-depleted (si53BP1) or RAP80-depleted (siRAP80) A549 cells. Shown are means \pm SEM of at least three independent experiments. Significance is indicated as ns for not significant, * for the $P < 0.05$, ** for $P < 0.001$.

Synergistic rescue of end resection in BRCA1-deficient cells upon co-depletion of RAP80 and 53BP1.

Since, co-depletion of 53BP1 and RAP80 caused a synergistic increase in end resection, we reasoned that this might lead also to a better rescue of end resection in BRCA1-deficient cells. To substantiate this, CRISPR-CAS technology was used to establish a stably RAP80 knock-out sub-clone from the A549 cells. Indeed, further depletion of 53BP1 in RAP80-knock-out cells led to a substantial increase in the number of recruited RPA (Fig. 4A) and RAD51 foci (Fig. 4B). BRCA1-knockdown significantly decreased the number of RPA (Fig. 4C) and RAD51 (Fig. 4D) foci in RAP80-knockout cells. However, these numbers were significantly higher compared to that upon depleting BRCA1 in control cells. Again synergistic increase in the IR-mediated recruitment of RPA and RAD51 upon further 53BP1 depletion in RAP80-knockout cells (Fig. 4C&D).

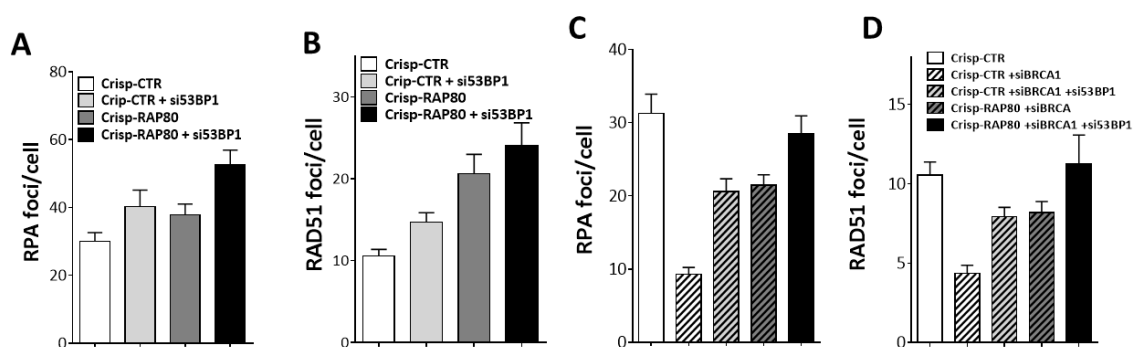


Fig. 4 Synergistic rescue of end resection in BRCA1-deficient cells upon co-depletion of RAP80 and 53BP1. CRISPR/CAS9 technology was used to create a RAP80-knock-out A549 subline. (A&B) 53BP1 was depleted in Crisp-CTR and Crisp-RAP80 clones before being irradiated 2Gy and RPA (A) and RAD51 (B) foci were then monitored after 2h and 4h post irradiation, respectively. (C&D) Quantification of RPA (C) and RAD51 (D) foci after depletion of 53BP1 and/or BRCA1 in Crisp-CTR or Crisp-RAP80 sub-clones. Shown are means \pm SEM of at least three independent experiments. Significance is indicated as ns for not significant, * for the $P < 0.05$, ** for $P < 0.001$.

These data were further recapitulated in BRCA1-deficient HCC1937 cells, indicating a restoration of HR activity in BRCA1-deficient cells upon RAP80 depletion. In order to test whether this drives a resistance to PARPi and or carboplatin-based drugs, the cellular survival after olaparib or MMC treatment was analyzed in BRCA1-depleted cells after further RAP80-knockdown. As illustrated in Fig. 5, the survival was rescued in BRCA1-depleted A549 cells upon downregulating either 53BP1 or RAP80 and more profoundly in double deficient cells. Collectively, these data (i) confirm the presence of a BRCA1-independent role for RAP80 in regulating DSB end resection and (ii) indicate RAP80 as a biomarker for the resistance to PARPi and MMC.

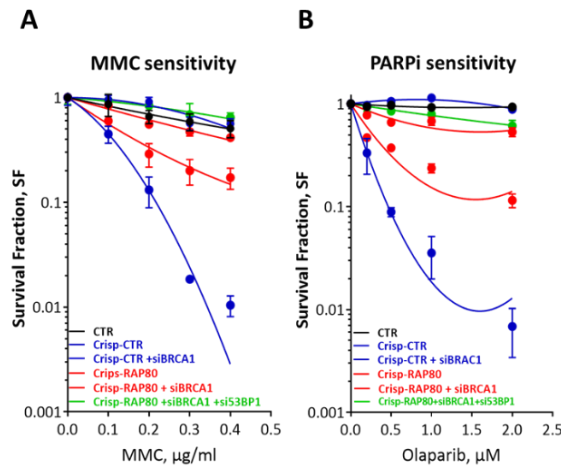


Fig 5. Loss of RAP 80 rescues the cell survival in BRCA1-deficient cells after MMC or PARPi treatment. Crisp-CTR or Crisp-RAP80 clones were depleted for BRCA1 and 53BP1 before the treatment with the indicated concentrations of MMC (A) or Olaparib (B) and survival fractions (SF) were measured by colony formation assay (CFA). Shown are means \pm SEM of at least three independent experiments.

Revealing the mechanism underlying the BRCA1-independent RAP80's role

Next, we sought to investigate the mechanism underlying the BRCA1-independent role of RAP80 in protecting DSB ends. During analysis of the RPA foci in RAP80 deficient cells, we observed that RPA foci seem to be bigger in size and more intense (Fig. 6A). Z-stacked immunofluorescence imaging was exploited to quantify RPA IRIF size and intensity in A549 cells depleted for 53BP1 or RAP80 before irradiation with 2Gy. Results revealed that the volume and intensity of RPA foci increased at least 3 times upon RAP80 knockdown compared to that upon 53BP1 depletion (Fig. 6B&C). In parallel experiments, CtIP or BRCA1 depletion resulted in a profound decrease in the number and size of RPA foci.

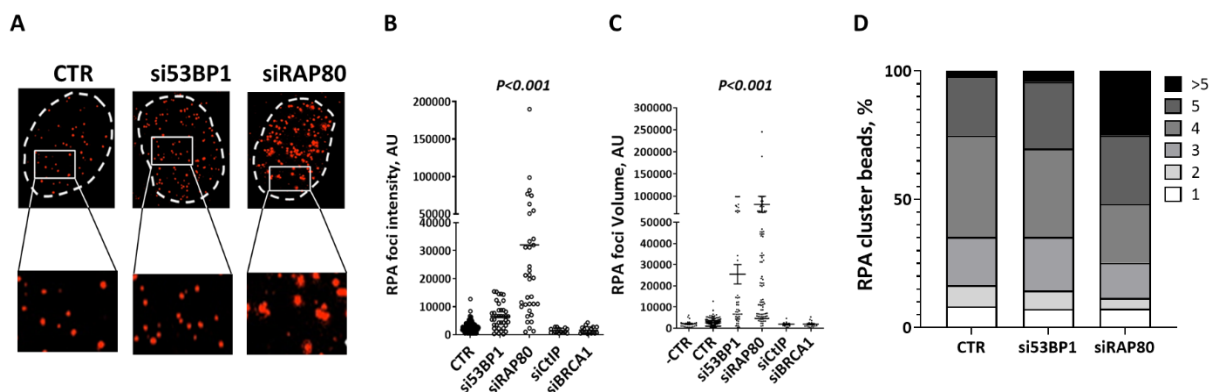


Fig. 6 RAP80 limits hyper-resection of DSB ends. Asynchronous A549 cells were treated with the indicated siRNA and RPA foci were monitored. (A) Representative IF images for the RPA foci in control (scRNA), 53BP1- (si53BP1) or RAP80-depleted (siRAP80) cells. RPA focus intensity (B) and volume (C) of about 2000 foci was measured at 2h post-2Gy A549 cells treated with the indicated siRNAs. Data presented as the mean \pm SEM of two independent experiments. (D) Quantification of RPA clusters visualized by electron microscopy consisting of the indicated number of beads, analyzed at 2h post-2 Gy in A549 cells pre-treated with the indicated siRNA.

As an independent assay to further investigate the RPA foci in RAP80-deficient cells, we employed the previously established gold-labeling based electron microscopic analysis for the localization of different DNA repair factors in irradiated cells. Using a RPA antibody for immunogold-labeling experiments, we demonstrated that after

irradiation, most of RPA foci were formed in up to 4 beads containing clusters (75.5%) in wild type cells. 23% of RPA foci were clustered in 4-5 beads and very few (2%) were clustered in more than 5 beads in wild type cells. In 53BP1-depleted cells, still most of RPA clusters consisted of up to 4 beads however with less percentage (69.5%). The number of RPA clusters with 4-5 beads was slightly higher (26%), but more importantly, the number of RPA clusters consisted of more 5 beads increased 2 folds reaching 4.3% in 53BP1-depleted cells (Fig. 6D). On the other hand, RAP80-deficient cells showed different distribution of the number of beads within RPA clusters. More importantly, a decrease in the number of RPA clusters with up to 4 beads (48%) and with 4-5 beads (26.4%) while a profound increase in the number of RPA clusters with more than 5 beads (25.3%) were reported in RAP80-deficient cells compared to either wild type or 53BP1-depleted cells. This indicates that the extent of DSB end resection were much more savage i.e. hyperresected in RAP80-deficient compared to 53BP1-depleted cells.

Together, these data suggest that RAP80 contributes to the suppression of exaggerated HR activity through (i) regulating the availability of BRCA1 to form a complex with CtIP which then initiates end resection step and (ii) limiting the extent of end resection in a BRCA1-independent manner.

RAP80 regulates the stability of EXO1 exonuclease

Based on the above findings, it is then plausible to suggest a scenario whereby RAP80 contributes to the regulation of the second step of end resection. In line with this, EXO1 levels declined with time in HEK-293 cells after treatment with 2Gy (Fig. 7A). In order to test whether RAP80 contributes to this, EXO1 expression was analyzed up to 8h post 2Gy in CRISPR-CAS9 mediated RAP80-knockout A549 cells and compared to their normal counterparts. Again the decline in EXO1 expression was seen in control A549 cells (Fig. 7B, upper panel) and EXO1 decrease appeared to be due to proteasomal degradation as this could be inhibited by treatment with the proteasome inhibitor MG-132 (Fig. 7B, middle panel). Importantly, we were intrigued to find that the time-dependent decline in EXO1 expression was inhibited in RAP80-knockout cells (Fig. 7B, lower panel). Since EXO1 is degraded by the ubiquitin-proteasome system and this degradation is compromised in the absence of RAP80, it is then conceivable that RAP80 prevents the ubiquitination of EXO1. Analysis of EXO1 ubiquitination revealed that while, EXO1 ubiquitination increased with time in response to IR in control cells, the levels of EXO1 ubiquitination were dramatically lower in RAP80 knockout cells (Fig. 7C). These results implicate a regulatory role for RAP80 in targeting EXO1 to proteasome degradation.

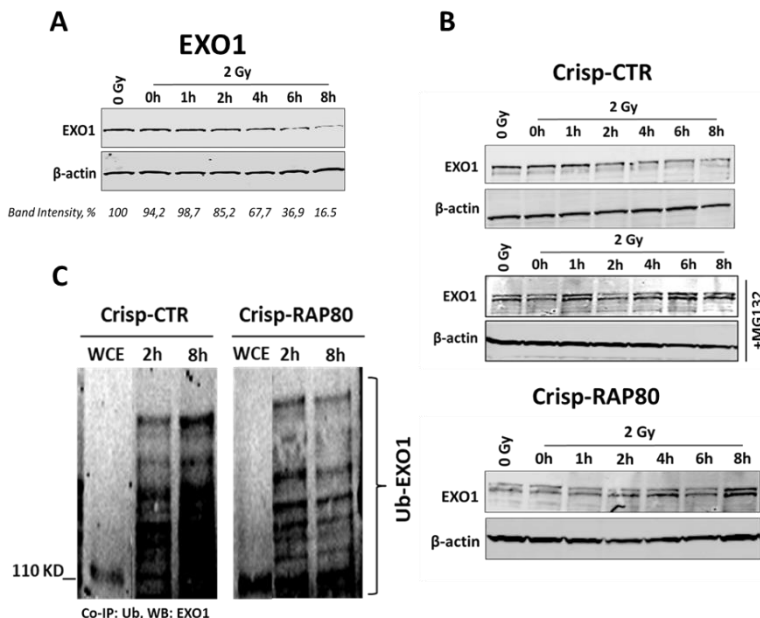


Fig. 7 RAP80 regulates the stability of EXO1 exonuclease. (A) Western blot showing the time-dependent EXO1 degradation in HEK293 cells. (B) EXO1 expression in after the indicated time points in CrispR-Cas control (Crisp-CTR) A549 cells before (upper panel) or after (middle panel) treatment with the proteasome inhibitor MG132. Lower panel shows the EXO1 expression in CrispR-Cas mediated RAP80-knockout (Crip-RAP80) A549 cells. (C) The indicated cells were ectopically transfected with a His6-ubiquitin expressing vector before being exposed to 2Gy. His6-ubiquitin-conjugated proteins were immunoprecipitated and ubiquitinated forms of EXO1 were detected by Western blotting.

In light of the apparent link between EXO1 degradation and RAP80, we sought to investigate whether RAP80 and EXO1 bind directly to each other. To that end, we co-expressed Flag-EXO1 and GFP-RAP80 in HEK-293 cells. GFP-RAP80 were captured and EXO1 was detected by Western blotting with anti-Flag antibody. Results reveal a binding between the two proteins (Fig. 8A). In order to examine the RAP80 domains required for the binding with EXO1, HEK-293 cells were co-transfected with Flag-EXO1 along with either GFP-RAP80-WT, or one of various RAP80 deletion mutants including GFP-RAP80-(1-204), GFP-RAP80-(1-304), GFP-RAP80-(1-404), or GFP-RAP80-(1-504) or GFP-RAP80- Δ UIM and examined their ability to interact with EXO1 by co-immunoprecipitation analysis. While, EXO1 was co-immunoprecipitated with RAP80 mutants outside the UIM domain, deletion of UIM domains prohibited the interaction between RAP80 and EXO1. This has also been verified after reversing the Co-IP upon co-transfecting HEK-293 cells with GFP-EXO1 and Flag- RAP80- Δ UIM and capturing the GFP-bound proteins and detecting the RAP80 by Western blot using anti-Flag antibody (Fig. 8A). Together, this indicates that EXO1 bind directly to RAP80 in an ubiquitination dependent manner through RAP80' UIM domains.

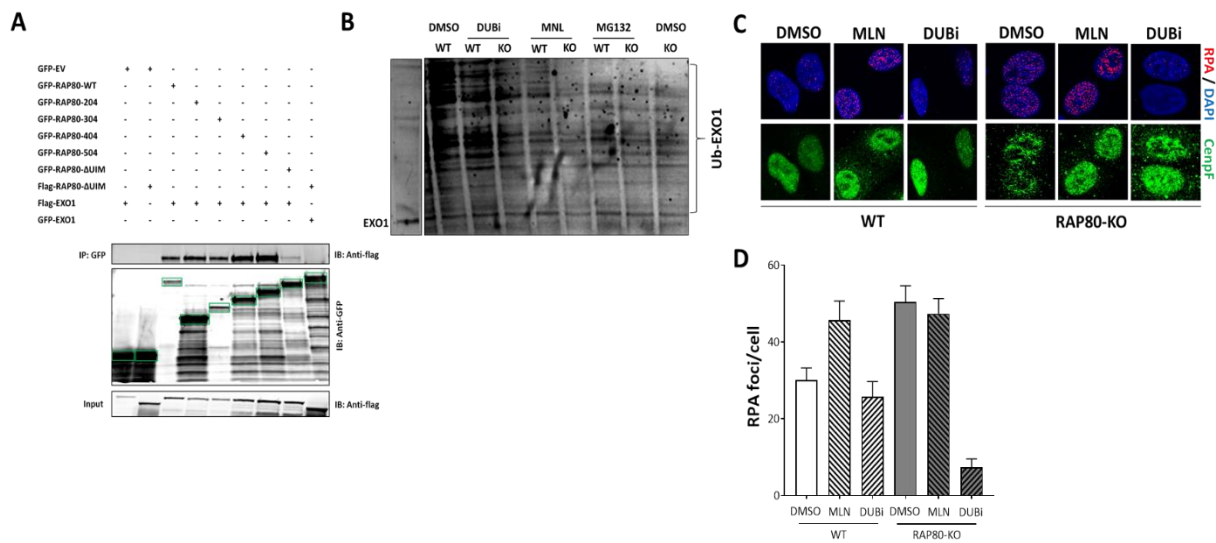


Fig. 7 RAP80 binds directly through its UIM domain to EXO1. (A) Co-immunoprecipitation analysis showing the direct binding between RAP80 and EXO1. In addition, this binding was only observable in case UIM domains are present. (B) Ubiquitination assay showing the extent of EXO1 ubiquitination upon treating either RAP80-wild type (WT) or RAP80-Knockout (KO) cells with the indicated inhibitors. (C) Representative images for RPA foci in WT vs RAP80-KO cells after the indicated treatment. (D) Quantification of the experiment represented in C. Shown are means \pm SEM of at least three independent experiments.

In order to test the effect of this ubiquitination on the regulation of RAP80-EXO1 axis, we inhibited cullin1 using the MLN inhibitor. As shown in Fig. 8B. MLN inhibitor as expected decreased EXO1 ubiquitination in WT but not in RAP80-KO cells. In consistency, a significantly enhanced end resection as indicated by increased the number of RPA foci in WT cells interestingly to comparable level of RAP foci numbers in RAP80-KO cells, while the end resection was not affected in RAP80-KO cells upon treatment with MLN inhibitor (Fig. 8C). Similar effects were also observed with the proteasome inhibitor MG-132 (Fig. 8B&C). These data revealed that inhibition of EXO1 ubiquitination and with that its stabilization in WT cells would mimic the situation in RAP80-lacking cells, indicating the importance of RAP80 in regulating the EXO1 stability through maintaining EXO1-ubiquitination by Cullin1.

Protein degradation is controlled by the opposing activities of ubiquitin ligases and deubiquitinating enzymes (DUBs). Therefore, it is deceiving to hypothesize that RAP80 prevents EXO1 deubiquitination by DUBs. To test this hypothesis, A549 cells were treated with xx μ M of xxx DUB inhibitor for 2h, which efficiently increased the EXO1-ub levels in RAP80-KO cells (Fig. 8B), before being irradiated with 2Gy and RPA foci were monitored in G2 cells at 2h post-irradiation. In keeping with our hypothesis, while the number of RPA foci was not affected in WT cells, it is significantly decreased in RAP80-KO cells upon treatment with DUBi (Fig. 8D).

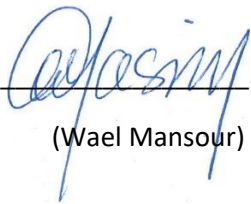
Conclusion

Collectively, our data propose a model explaining the role of RAP80 in regulating end resection. RAP80 binds to BRCA1, preventing its binding with the endonuclease CtIP. In addition, through its UIM domains, RAP80 interacts with ubiquitinated EXO1 to prevent its deubiquitination by a yet unidentified DUB. The polyubiquitinated EXO1 is then targeted to proteasome degradation, hence preventing the hyperresection of a DSB. Therefore, in RAP80-deficient cells, ubiquitinated chains on EXO1 are removed by a DUB, leading to its stabilization and with that DSB hyperresection.

The current study added another level of regulation of EXO1-mediated DSB end resection as a decisive step for appropriate pathway choice and maintaining genomic stability. Furthermore, it identifies RAP80 along with other identified factors as markers for the acquired PARPi resistance.

From the current data, a paper is being written, describing a novel role for RAP80 in DNA double strand break end resection through targeting EXO1 to proteasome degradation. This paper is planned to be submitted to Nucleic Acids Research (IF12).

Hamburg, den 29.09.2020



(Wael Mansour)